Function of SLAM-Associated Protein (SAP) in Acute Pneumoseptic Bacterial Infection

Jitendra K. Tripathi †, **Atul Sharma** †, **Kuldeep Gupta, Houda Abdelrahman, Pooja Chauhan, Bibhuti B. Mishra and Jyotika Sharma**

Department of Biomedical Sciences, *The University of North Dakota School of Medicine and Health Sciences, 1301 N Columbia Road, Grand Forks, ND 58202-9037, USA*

Correspondence to Jyotika Sharma: *Department of Biomedical Sciences, The University of North Dakota School of Medicine and Health Sciences, 1301 N Columbia Road, Grand Forks, ND 58202-9037, USA.*
jyotika.sharma@med.und.edu
https://doi.org/10.1016/j.jmb.2019.07.002
Edited by Shabaana Abdul Khader

Abstract

Sepsis resulting from acute pneumonic infections by Gram-negative bacteria is often characterized by dysfunction of innate immune components. Here we report a previously unrecognized innate protective function of SAP, an adaptor protein primarily reported in T cells, NK cells, and NKT cells, during acute pneumonic infection with *Klebsiella pneumoniae* (KPn). SAP-deficient mice were highly susceptible to this infection with elevated systemic bacterial spread and increased lung damage. While the overall influx of infiltrating cells in the lungs remained largely intact, increased mortality of SAP-deficient mice correlated with increased accumulation of large NK1.1+ cells harboring bacteria and an impairment of neutrophil extracellular trap formation *in vivo* during KPn pneumonia, which likely facilitated bacterial outgrowth. Neutrophils were found to express SAP; however, adoptive transfer experiment supported a neutrophil-extrinsic function of SAP in neutrophil extracellular trap formation. Collectively, these data present the first report depicting innate protective function of SAP in an acute pulmonary infection.

Introduction

Despite significant advances in understanding of immune mechanisms, pneumonic sepsis remains a major healthcare concern [1,2]. Nosocomial infections caused by Gram-negative pathogens such as *Klebsiella pneumoniae* (KPn) are especially concerning due to an alarming increase in the antibiotic resistance of this pathogen [3]. Because the combined arsenal of immunomodulatory and antimicrobial factors deployed by neutrophils and macrophages plays a critical role in clearance of infectious insults, innate immune dysfunctions related to these cells are major contributors to morbidity and mortality associated with sepsis [4]. Neutrophil extracellular trap (NET) formation is a newly described mechanism by which neutrophils trap and kill pathogens extracellularly [5,6]. While the protective function of NETs in infectious septic conditions is increasingly recognized, molecular underpinnings of this fascinating paradigm of neutrophil activation are only beginning to unravel. Thus, identification of new and novel signaling components regulating these innate immune functions can thus provide new therapeutic targets to treat sepsis by boosting neutrophil and macrophage functions in a clinical setting.

Signaling lymphocytic activation molecule (SLAM)-associated protein (SAP) is an SH2 domain-containing adaptor protein that regulates signaling events downstream of the SLAM-family receptors expressed by hematopoietic cells [7]. SAP facilitates SLAM receptor signaling to regulate Th2 differentiation [8], iNKT cell development [9], and B-cell differentiation [10]. In humans, loss of function mutations in Sh2d1a gene-encoding SAP results in heritable X-linked lymphoproliferative disease (XLP-1), which is characterized by increased susceptibility of immunodeficient males to fulminant infectious mononucleosis

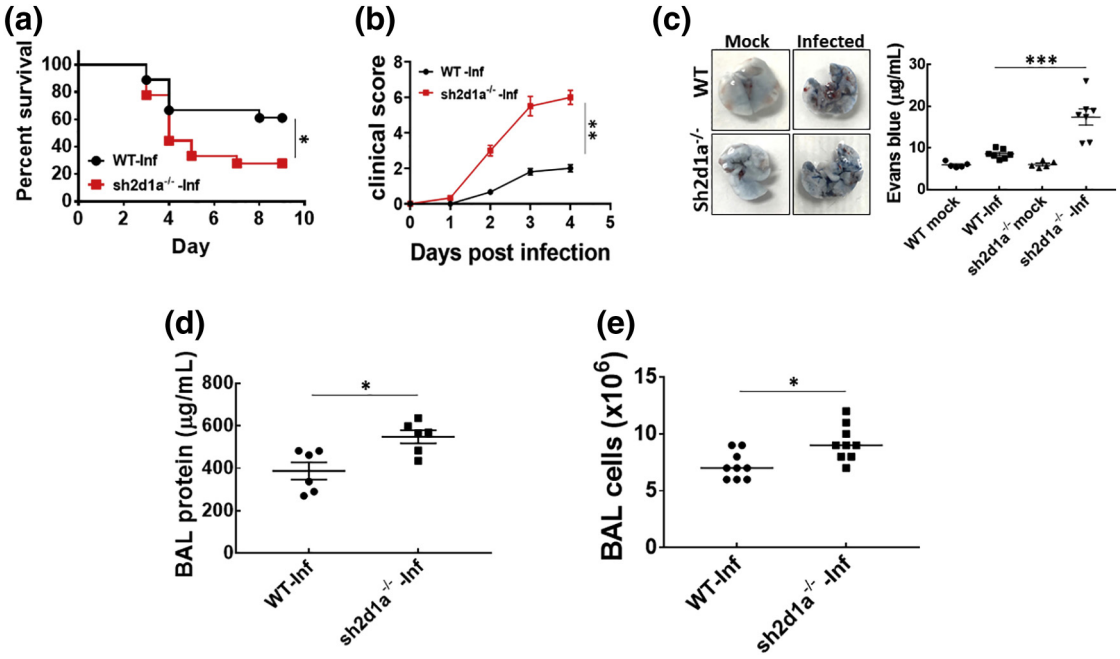

Fig. 1. SAP-deficient mice display increased mortality during acute pneumoseptic infection with *K. pneumoniae*. (a) WT- and SAP-deficient sh2d1a$^{-/-}$ mice were intranasally infected with KPn, and disease progression was assessed daily for 10 days. Statistical comparison of mortality was made using the Kaplan–Meier survival curve (*$p < 0.05$). The data shown are from three independent experiments (n = 18/group). Clinical scores (b), lung vascular and epithelial damage (c), total protein in the BALF (d), and total number of infiltrating cells in the BALF (e) of KPn-infected WT (WT-Inf) and sh2d1a$^{-/-}$ (sh2d1a$^{-/-}$-Inf) assessed as described in Materials and Methods. n = 6–7 each group. Data are mean ± SEM. Statistical comparisons done by Student's *t* test: *$p < 0.05$, **$p < 0.01$, ***$p < 0.001$.

resulting from Epstein–Barr virus infection [11]. Although SAP can interact with cytosolic tyrosine-based switch motifs of various SLAM receptors, including those regulating effector functions of phagocytes [12], there is little information on expression and direct role of SAP in innate immune cells. Moreover, whether this protein contributes to innate immunity during acute bacterial infections is completely unknown.

In this study, we tested the role of SAP in Gram-negative pneumoseptic infection of mice by KPn. Our results show that SAP mitigates mortality and associated lung damage in acute pulmonary KPn infection and regulates innate immune cell functions. Our findings present a new function of SAP, which may be a drug-able target in pneumonic sepsis and NET-related pathologies.

Results and Discussion

Increased susceptibility of sh2d1a$^{-/-}$ mice to pneumonic KPn infection

In our continued efforts to understand the pathogenesis of pneumoseptic infection with KPn, we sought to examine if SAP plays any role in the process. For this, we first examined if SAP-deficient sh2d1a$^{-/-}$ and WT mice respond to pulmonary KPn infection differentially. Upon intranasal infection with an experimentally determined sublethal dose of KPn, 60%–65% of WT mice survived the infection with significantly lower clinical scores (Fig. 1a and b). The sh2d1a$^{-/-}$ mice, on the other hand, were highly susceptible to the infection, and 80% of the mice succumbed to infection within 7 days with progressive development of disease. While the disease signs appeared similar in WT and sh2d1a$^{-/-}$ mice initially, the knock-out (KO) mice exhibited significantly elevated clinical scores by 2 days post-infection (dpi) with maximum difference observed at 3 dpi (Fig. 1b). This is in line with our previous reports showing 3 dpi to be the peak of pneumoseptic KPn infection [13–15]. Accordingly, we found significantly higher lung damage in infected sh2d1a$^{-/-}$ mice at 3 dpi, as determined by increased epithelial and vascular permeability (Fig. 1c), elevated protein levels in the airways (Fig. 1c), and increased overall cellular infiltration in the lungs (Fig. 1e). To compare the overall lung pathology, hematoxylin and eosin-stained slices of the lungs isolated at various times post-infection were analyzed. As shown in Fig. 2a, mock control WT and sh2d1a$^{-/-}$ mice displayed similar normal lung tissue morphology. Infected WT mice exhibited pronounced areas of perivascular and peribronchial infiltration in the lungs

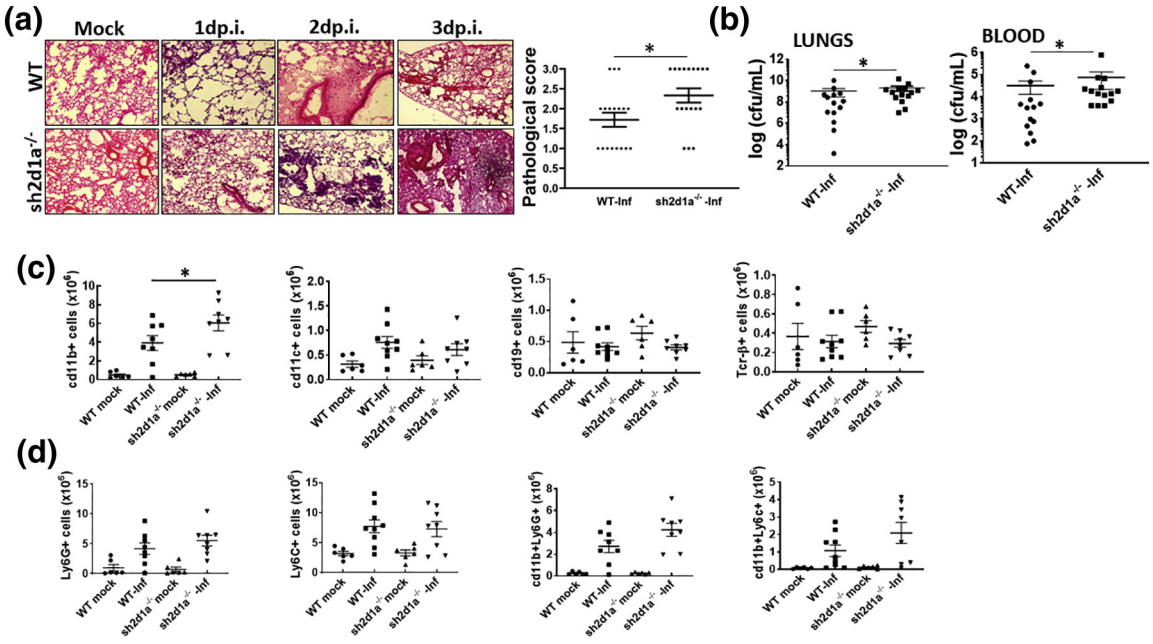

Fig. 2. Pneumonic sh2d1a$^{-/-}$ mice exhibit severe lung pathology and impaired bacterial control. (a) Histopathological assessment by hematoxylin and eosin staining of lung cryosections obtained from mock control and KPn-infected WT and sh2d1a$^{-/-}$ mice at 1, 2, and 3 dpi. Representative images from six mice per group in three independent experiments are shown. Graph shows 4-point manual pathological score (described in Materials and Methods) of the lungs at 3 dpi. Data are mean ± SEM. *$p < 0.05$. (b) Bacterial burden in the lungs and blood of KPn-infected WT and sh2d1a$^{-/-}$ mice at 3 dpi. Data are pooled from three independent experiments; each dot represents one mouse (n = 4–5 each group/experiment). (c and d) Flow cytometry quantitation of leukocytes in the lungs of KPn-infected WT and sh2d1a$^{-/-}$ mice at 3 dpi. Data shown in scatter plots are pooled from three independent experiments (n = 2–3 per group for each experiment). Each dot represents one mouse. *$p < 0.05$.

at 2 dpi. Despite an increased immune cell influx at 3 dpi, the overall lung architecture was preserved in the WT mice throughout the infection. The sh2d1a$^{-/-}$ mice on the other hand displayed an earlier elevated cellular influx at 1 dpi, which increased through the course of infection. By 3 dpi, the KO lungs exhibited substantial foci of consolidation, bronchial wall thickening, and airspace occlusion. Pathological scoring of the lungs using these criteria confirmed that sh2d1a$^{-/-}$ mice exhibited significantly worse lung pathology as compared to the WT mice (Fig. 2a, scatter plot).

To examine whether the bacterial clearance was compromised due to increased lung damage, we compared local and systemic bacterial loads in WT and sh2d1a$^{-/-}$ mice. In the WT mice, the bacterial burden data obtained in the lungs and blood were found to be spread widely, which likely reflected the range of progression of infection in sick and recovering mice (Fig. 2b). Majority of sh2d1a$^{-/-}$ mice, on the other hand, exhibited similar overwhelming bacterial loads locally in their lungs and systemically in blood with much reduced spread of the data compared to WT mice. Together with the survival and lung pathology, these data suggest that KPn infection induced severe lung pathology and increased local outgrowth of bacteria resulting in higher systemic spread and increased mortality. In order to examine which immune cell types likely contributed to disease severity in sh2d1a$^{-/-}$ mice, we profiled immune cell infiltrates in the lungs of KO and WT mice at 3 dpi by flow cytometry. The most strongly modulated cell population was found to be CD11b+ myeloid cells, which were significantly increased in the sh2d1a$^{-/-}$ mice compared to the WT mice at 3 dpi (Fig. 2c). There were no significant differences between the infected WT and KO lungs in the numbers of dendritic cells, B cells, and T cells. Compared to the mock controls, an infection-induced reduction in B- and T-cell numbers in both WT and sh2d1a$^{-/-}$ mice was observed, which is in line with the lymphocyte depletion characteristic of sepsis, reported by us and others [16–18]. These data also support an innate function of SAP in this acute bacterial infection, since SAP deficiency causes a hyperproliferation of T cells in chronic disease conditions [19]. In light of the increased numbers of CD11b+ cells in the lungs of sh2d1a$^{-/-}$ mice, we further characterized these cells by co-analyzing the expression of CD11b with granulocytic/monocytic markers Ly6G and Ly6C. The KPn-infected sh2d1a$^{-/-}$ mice exhibited a moderate but non-significant increase in Ly6G+ granulocytes and CD11b+ Ly6G+ neutrophils compared to their WT

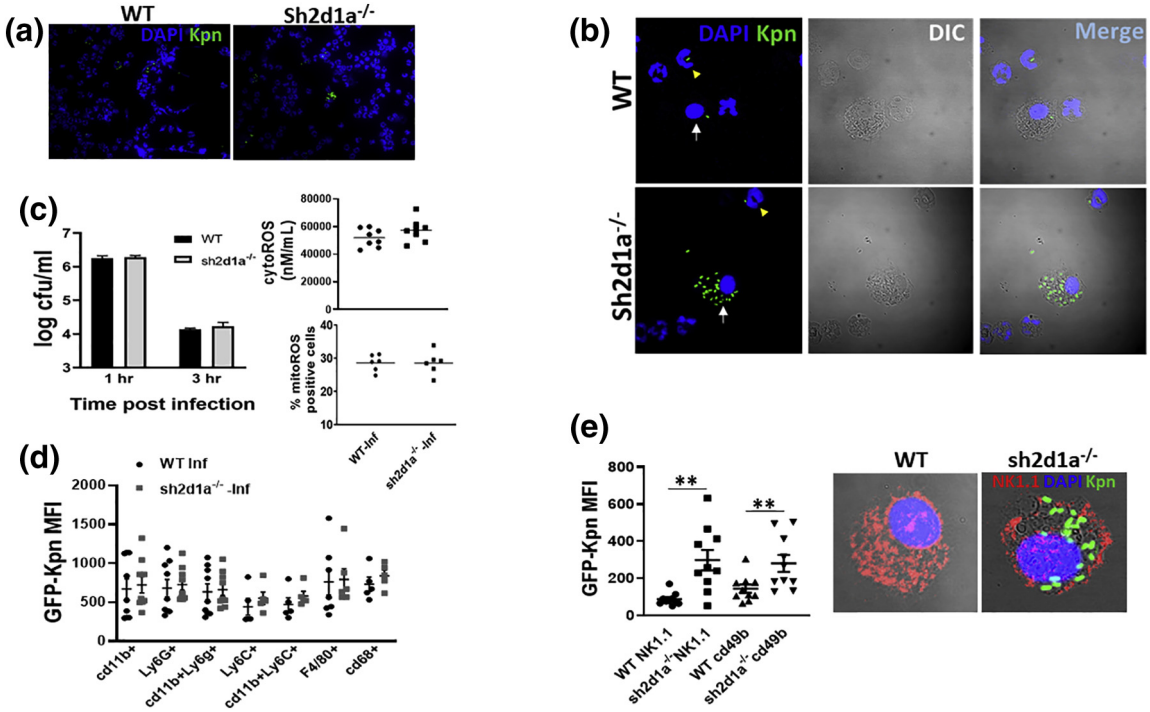

Fig. 3. SAP regulates immune cell functions in the lungs during KPn infection. (a) BAL cells isolated from WT or Sh2d1a$^{-/-}$ mice infected with GFP-Kpn were cytocentrifuged on glass slides and mounted with ProLong Diamond Antifade Mountant with DAPI (Invitrogen). The images were acquired using Nikon Eclipse 80I fluorescence microscope. Magnification 400×. (b) Higher magnification of panel A depicting neutrophils (yellow arrowheads) and large infiltrating-like cells frequently harboring high bacterial load (white arrows). (c) Bacterial uptake and killing capacity of sh2d1a$^{-/-}$ and WT neutrophils was determined at 1 and 3 h by assessing intracellular colony-forming units in these cells as described in Materials and Methods. Data from a representative of three independent experiments are shown. Cytosolic (CytoROS) and mictochondrial (mitoROS) reactive oxygen species were measured in BAL neutrophils isolated from KPn-infected WT (WT-Inf) and sh2d1a$^{-/-}$ (sh2d1a$^{-/-}$-Inf) as described in Materials and Methods. Data shown are two independent experiments with three to four mice each group per experiment. Each dot represents one mouse. The horizontal line in the graph is the mean of the represented value. (d) BAL cells isolated from WT or Sh2d1a$^{-/-}$ mice infected with GFP-Kpn were analyzed by flow cytometry using indicated myeloid cell markers. Mean fluorescence intensity of GFP-KPn in various cell types is shown. Data shown are pooled from three independent experiments with two to four mice each group. Each dot represents one mouse. (e) BAL cells isolated from WT or Sh2d1a$^{-/-}$ mice infected with GFP-Kpn were analyzed by flow cytometry or IF staining using NK cell markers. Magnification 600×. Data shown are pooled from three independent experiments with three to four mice each group. Each dot represents one mouse. IF images are representative of two independent experiments. Images were acquired using Zeiss LSM-510 Meta Confocal Microscope.

counterparts (Fig. 2d). The numbers of Ly6C+ monocytes did not change during infection, while CD11b+Ly6C+ cells exhibited a non-significant increase in the lungs of the infected sh2d1a$^{-/-}$ compared to WT mice. Representative dot plots for flow cytometry analysis of various cell types are shown in Supplementary Fig. 1.

Because flow cytometry with a defined panel of cell markers yielded little information on specific immune cell type that could account for the increased lung pathology and higher bacterial burden, we sought to examine the morphological features of immune cells infiltrating into the lungs of KPn-infected sh2d1a$^{-/-}$ and WT mice. For this, mice were infected with GFP-tagged fluorescent KPn, and the lungs were lavaged at 3 dpi. The bronchoalveolar lavage (BAL) cells were cytocentrifuged and analyzed. As shown in Fig. 3a, neutrophils with characteristic multi-lobed nuclei were found to be the most abundant infiltrating cell type in sh2d1a$^{-/-}$ and WT lungs. This was in line with the flow cytometry data showing myeloid cells expressing CD11b+ and Ly6G+ to be the predominant cell type in both WT and sh2d1a$^{-/-}$ compared to other immune cells (Fig. 2c and d). In both KO and WT mice, the neutrophils were found to harbor one to two fluorescent bacteria, indicating that SAP deficiency does not interfere with the bacterial uptake and intracellular killing capacity of neutrophils (Fig. 3a and b, yellow arrowheads). This was supported by a similar bacterial uptake and killing as well as production of reactive oxygen species by neutrophils from WT and the KO mice (Fig. 3c). Interestingly, we observed a substantial number of large, vacuolated, cells in the BAL of sh2d1a$^{-/-}$ mice, which frequently harbored a

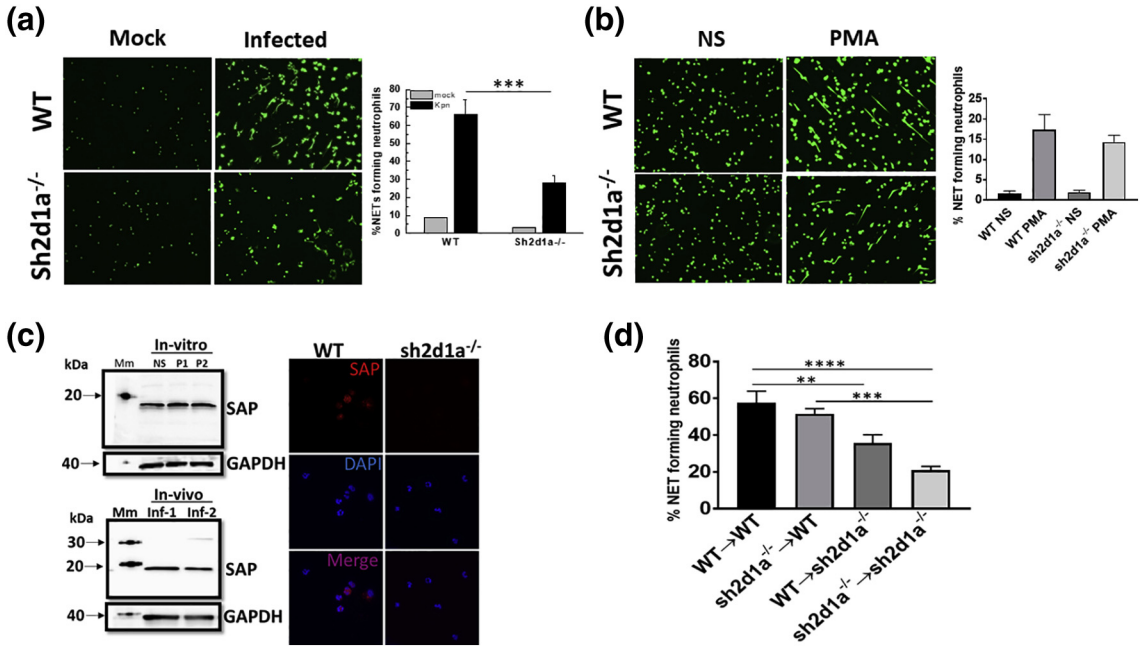

Fig. 4. Impaired NET formation in the absence of SAP. (a) BAL cells isolated from mock control (PBS alone) or KPn-infected WT and sh2d1a$^{-/-}$ mice at 3 dpi and cytocentrifuged on glass microscope slides. NETs were fixed and stained with DNA dye Sytox Green as described in Materials and Methods. Representative fluorescence images from three independent experiments are shown (magnification 200×). The bar graph shows the average ± SEM of NETs counted from three independent experiments. ***$p < 0.001$. (b) Representative fluorescence images of NETs in WT and sh2d1a$^{-/-}$ peritoneal neutrophils unstimulated (NS) or stimulated with PMA (100 nM) for 4 h. NETs were visualized using Sytox Green. Magnification 200×. The bar graph shows quantitation of NET forming WT and sh2d1a$^{-/-}$ neutrophils. Data presented in the bar graph are average ± SEM from three independent experiments. No statistically significant difference in NET formation was found between PMA stimulated WT and sh2d1a$^{-/-}$ neutrophils. (c) Western blot analysis to detect expression of SAP protein in WT peritoneal neutrophils upon PMA stimulation *in vitro* for 10 min (P1) or 30 min (P2), or in BAL neutrophils isolated from WT mice infected with KPn for 3 days (*in vivo*). SAP expression in BAL neutrophils of two mice (Inf-1 and Inf-2) from one experiment representative of two performed is shown. Mm denotes molecular weight marker. Right panel shows representative IF images of SAP expression (red) in WT BAL neutrophils stained with anti-SAP antibody. Nuclei were stained with DAPI. BAL neutrophils from sh2d1a$^{-/-}$ mice were used as negative control. Magnification 400×. (d) Adoptive transfer of cell tracker orange CMRA dye-labeled WT or sh2d1a$^{-/-}$ neutrophils in the lungs of mice was performed as described in Materials and Methods. Four hours after transfer, BAL cells were isolated from each mouse, cytocentrifuged on microscopic glass slides, and fixed with 4% paraformaldehyde followed by Sytox Green nuclear staining (100 nM). Images were acquired using Olympus IX83 TIRF Fluorescent Microscope and processed by Image J software. The percent NET formation in each group was manually quantitated by dividing the number of the adoptively transferred (dye-labeled) NET-forming neutrophils by the total number of adoptively transferred neutrophils in 8–10 random microscopic fields and multiplying the values by 100. Various groups denote WT or KO neutrophils transferred to WT or KO lungs. Data presented in the bar graph are from three independent experiments. Statistical analysis done by one-way ANOVA multiple-comparisons test: **$p < 0.01$, ***$p < 0.001$.

large number of bacteria (Fig. 3b, arrows). Flow cytometry analysis of GFP KPn-positive cells using various monocytic/macrophage markers did not reveal any difference in the numbers of these cells in BAL from infected WT and KO mice (Fig. 3d). Since SAP has been implicated in antimicrobial functions of NK cells [20] and a protective function of NK cells is shown in KPn infection [21], we analyzed these cells using NK cell markers. Indeed, NK1.1+ and CD49b+ cells were found to harbor significantly higher GFP-Kpn in sh2d1a −/− BAL as compared to their WT counterparts (Fig. 3e). NK cells are large, granular, innate lymphocytes predominantly recognized for their cytotoxic defense against tumor and virally infected cells [22]. While the receptor-mediated cytotoxicity toward infected cells is the most well-characterized functions of NK cells, recent evidence shows that NK cells can directly bind to bacteria and parasites [23]. While pathogen uptake by NK cells as a result of this interaction was not examined in these studies, actin-dependent phagocytosis of *Candida albicans* by activated NK cells has been reported [24]. Our unexpected finding of sh2d1a$^{-/-}$ NK1.1+ cells harboring KPn is in line with these reports and implicates that SAP in NK1.1+ cells mediated uptake of KPn. It remains to be tested whether these are NK cells defective in degranulation and serve as a replicative niche for KPn to aid in systemic spread of

the pathogen. It is also interesting to note here that neutrophils have been reported to prevent NK cell activation [24]. Whether the relatively higher numbers of neutrophils in sh2d1a$^{-/-}$ mice, as reported here, contribute to inhibition of NK1.1+ cells activation, if any, and the role of SAP in NK1.1+ cells activation and their interaction with myeloid cells during KPn infection are currently ongoing in our laboratory.

Reduced NET formation in the absence of SAP

We have previously reported a protective, antimicrobial function of NETs, which are DNA fibrils coated with various proteins with antimicrobial activity, in KPn infection [6,14]. In order to assess the role of SAP in NET formation, the lungs of the infected WT and KO mice were lavaged at 3 dpi, followed by quantitation of NETs in cytocentrifuged BAL cells. As shown in Fig. 4a, sh2d1a$^{-/-}$ mice exhibited significantly reduced NET formation in-lungs during KPn infection as compared to the WT mice. In contrast to this *in vivo* impairment of NET formation during infection, sh2d1a$^{-/-}$ neutrophils were found to be fully competent in NET formation *in vitro*, in response to neutrophil activating compound phorbol myristate acetate (PMA; Fig.4b). This suggested that SAP plays a role in the lung microenvironment to induce NETs and prompted us to examine if neutrophil extrinsic or intrinsic function of SAP was required for NET formation *in vivo* during KPn infection. To the best of our knowledge, SAP expression in neutrophils has never been reported. We thus first examined if neutrophils express SAP during KPn infection and PMA stimulation. Western blot analysis showed similar baseline and activation-induced expression of the 15-kDa SAP protein in unstimulated and PMA-stimulated WT neutrophils (Fig. 4c, upper left panel). The duration of PMA stimulation (10 or 30 min) did not increase the SAP amount. A similar expression of SAP was observed in BAL neutrophils isolated from KPn-infected WT mice (Fig. 4c, lower left panel). immunofluorescence (IF) staining showed abundant expression of SAP distributed in the cytosol of BAL neutrophils isolated from KPn-infected WT mice at 3 dpi (Fig. 4c, right panel). An absence of staining in sh2d1a$^{-/-}$ neutrophils confirmed the specificity of the anti-SAP antibody used. After confirming SAP expression in neutrophils, an adoptive transfer experiment was performed to dissect the role of neutrophils extrinsic or instrinsic role of SAP in NET formation. Bone marrow neutrophils purified from sh2d1a$^{-/-}$ or WT mice were labeled with fluorescent dye CMRA, as described in Materials and Methods, and were inoculated intranasally in KPn-infected WT or SAP KO mice at 2 dpi. This ensured the infection-induced generation of any factors possibly playing a role in NET formation. The lungs were lavaged 4 h and after transfer of labeled neutrophils, cytocentrifuged, and NET formation in fluorescent dye-labeled neutrophils was quantified. In line with our previous observation, sh2d1a$^{-/-}$ neutrophils instilled in sh2d1a$^{-/-}$ mice exhibited significantly reduced NET formation when compared to WT neutrophils instilled in WT mice (Fig. 4d). Importantly, sh2d1a −/− neutrophils exhibited similar NET formation when transferred in WT lungs. This restoration of NET formation capacity of sh2d1a$^{-/-}$ neutrophils in WT lung environment suggested that neutrophil-extrinsic factors present in the lung microenvironment during KPn infection influence NET formation in the absence of SAP. This was further confirmed by a significantly reduced NET formation in WT neutrophils transferred in lungs of sh2d1a$^{-/-}$ mice. Despite the expression of SAP in neutrophils, a neutrophil-extrinsic effect of this protein on NET formation suggests that SAP-mediated functions in other cell types in lung microenvironment likely modulate NET formation. Given our data discussed above and other studies showing the role of SAP in NK1.1+ cells functions, it is tempting to speculate that direct (receptor mediated) or indirect (cytokine secretion) interaction of NK1.1+ cells with neutrophils possibly affects NET formation during KPn infection.

Taken together, we report here for the first time a protective function of SAP in pneumoseptic bacterial infection. We show that in the absence of SAP, mice are more susceptible to pulmonary KPn infection with severe lung damage and increased lung and systemic bacterial loads. Reduced bacterial clearance in SAP-deficient mice correlated with increased numbers of NK1.1+ cells harboring bacteria and an impaired NET formation, despite an intact bacterial uptake and oxidative burst in neutrophils, the main cell-type implicated in control of KPn. Of relevance, an antimicrobial function of NETs in KPn infection has been demonstrated by us [6]. Although speculative at this stage, impairment of NK1.1+ cells functions in the absence of SAP, which in turn can activate multiple cell types to coordinate a protective immune response during infection [25], also likely contributes to increased susceptibility of sh2d1a −/− mice. Taken together, our study opens up a new area of research on this adaptor protein and NK1.1+ cells functions in *Klebsiella* pathogenesis.

Materials and Methods

Antibodies

Antibodies used for flow cytometry include Pacific Blue anti-mouse CD11b (clone M1/70), allophycocyanin-Cy7 anti-mouse CD11c (clone N418), FITC anti-mouse CD19 (clone 6D5), allophycocyanin anti-mouse Ly6G (clone 1A8), PerCP-Cy5.5 anti-mouse

Ly6C (clone HK1.4), PE-Cy7 anti-mouse F4/80 (clone BM8) (all from BioLegend, San Diego, CA), and PE anti-mouse TCR-β (clone H57-597) Ab (BD Pharmingen,San Jose, CA), APC anti-mouse NK1.1 (clone PK136), PE anti-mouse CD49b (clone HMα2), Brilliant Violet 605™ anti-mouse CD68 Antibody (clone FA-11). Anti-SH2D1A/SAP antibody (abcam -ab185810) and GAPDH (Goat polyclonal Antibody Genscript A00191), which were used for Western blot and IF microscopy.

Infection of mice and survival

Age- and sex-matched wild-type C57BL/6 (WT) and SAP-deficient (sh2d1a$^{-/-}$) mice (kindly provided by Dr. Pamela Schwartzberg, NHGRI, NIH) bred in the animal facility of the University of North Dakota were used according to institutional and federal guidelines. Phenotypic characterization of sh2d1a$^{-/-}$ mice has revealed no homeostatic abnormalities [26]. Mice were infected intranasally with 3×10^4 bacteria in 20 μl of saline of KPn (ATCC strain 43816). For some experiments, GFP-labeled KPn (Kindly provided by Dr. Stephen Clegg, Iowa) was used for infection. Mock-infected mice received saline only. Mice were monitored daily for signs of disease, and mortality was recorded for up to 10 dpi as described previously [6,13,14].

Bacterial burden, clinical scoring, and histological analysis

Serial dilutions of aseptically homogenized lungs and blood from infected and mock control (PBS inoculated) mice were plated on LB agar. Colony-forming units were counted after overnight incubation at 37 °C. Disease progression was assessed using a clinical scoring system that assigned one point each to piloerection, hunched gait, labored breathing, movement (decreased, only on provocation, or absent), and eye discharge. For histological analysis, snap-frozen lungs in OCT resin were processed into 10-μm-thick serial horizontal sections and stained with hematoxylin and eosin as described previously by us [6,13,14,27]. A 4-point pathological scoring system was used, which assigned 0 for the normal architecture, 1 for the progressive thickening of alveolar septa and decrease of alveolar space, 2 for increase in alveolar septal thickening and decrease in alveoli space with inflammatory cells invasion, and 3 for extensive damage of tissue architecture.

Measurement of pulmonary vascular permeability

Vascular and pulmonary epithelial damage in infected WT and sh2d1a$^{-/-}$ mice was quantified as described [28]. Briefly, mice were injected intraperitoneally (i.p.) with Evans blue dye (0.2 ml of 0.5% in PBS). Four hours after injection, the lungs were harvested following perfusion with PBS, and the dye was extracted in Formamide (Sigma-Aldrich) overnight at 55 °C. Evans blue dye concentrations were quantified against a standard curve by measuring absorbance at 610 nm with deduction of reference absorbance at 450 nm. Airway protein was quantified by BCA protein assay (Thermo Scientific) in cell-free bronchoalveolar lavage fluid (BALF) recovered by methods described previously by us [6,14,29].

Western blot and IF microscopy

To examine the expression of SAP in neutrophils *in vitro*, WT peritoneal neutrophils were stimulated with PMA (100 nM) for 10 or 30 min. Cells were lysed with RIPA buffer containing protease and phosphatase inhibitors. Lysates were loaded on SDS-PAGE gels and transferred to polyvinylidene difluoride membranes, and the blots were probed with Anti-SH2D1A/SAP antibody (abcam -ab185810). GAPDH (Goat polyclonal Antibody Genscript A00191) was used as loading control. Immunoreactivity was detected using super signal west Pico plus Chemiluminescent substrate (Thermo Scientific) and analyzed on Bio Rad reader using Quantity one software and Chemi doc scanner. To examine the expression of SAP in in vivo condition, BALF was recovered from KPn-infected WT mice at 3 dpi. Cells were then processed for Western blot analysis as described above.

IF staining was performed using standard protocols as previously described by us [30,31]. For detection of SAP protein, BAL cells isolated from KPn-infected WT and sh2d1a$^{-/-}$ mice at 3 dpi were cytocentrifuged on glass slides and fixed with 4% paraformaldehyde. Immunostaining was performed using anti-SH2D1A/SAP antibody followed by Alexa Fluor 546 conjugated goat anti-rabbit secondary antibody (Thermo fisher scientific inc. USA). For GFP Kpn imaging, the BAL cells isolated from WT or sh2d1a$^{-/-}$ mice at 3 dpi were cytocentrifuged on glass slides and mounted with ProLong Diamond Antifade Mountant with DAPI (Invitrogen). For the confirmation of natural killer cells by IF microscopy, cytocentrifuged cell were stained with APC anti-mouse NK1.1 The images were acquired using Zeiss LSM-510 Meta Confocal Microscope. Acquired image was processed by NIH ImageJ software.

Flow cytometry

For enumeration of immune cells, the lungs from mock control and infected animals isolated 3 dpi were processed to obtain total cellular infiltrates as previously described by us [13–15]. Cells were pre-incubated with Fc Block in PBS and Live/Dead Stain (Life Technologies), followed by incubation with fluorochrome-labeled antibodies for various cell

markers. A BDLSR II (BD Biosciences) flow cytometer was used for data acquisition, and FlowJo software (Tree Star) was used to analyze all data.

Bacterial phagocytosis and killing

Peritoneal neutrophils (5×10^5) from WT C57BL/6 and Sh2d1a$^{-/-}$ mice were incubated with KPn (MOI of 50) for 1 h to determine bacteria uptake and 3 h to determine bacteria killing. After 1 h, the cells were washed two times with warm PBS and one time with RPMI before adding 2 μg/ml gentamicin in RPMI (Gibco) with 10% FBS for the remaining 2 h (for the 3 h samples) and for 15 min for the 1-h samples. The cells were washed extensively with warm PBS before lysing with 0.1% TritonX100. Serial dilutions of the lysates were plated on LB media overnight at 37 °C before colonies were counted.

Neutrophil oxidative burst and NET formation

Reactive oxygen species in BAL neutrophils were measured by detecting hydrogen peroxide using the Fluoro H_2O_2 detection kit (Cell Technology) as per the manufacturer's instructions. For mitochondrial ROS measurement, BAL neutrophils were suspended in Hank's balanced salt solution and incubated for 10 min with MitoSOX Red Mitochondrial Superoxide Indicator (5 μM). Cells were then washed with Hank's balanced salt solution and analyzed by flow cytometry. Analysis and quantitation of NET formation *in vitro* (PMA stimulation) and *in vivo* (KPn infection) was done as described by us [6,13,14,29].

Adoptive transfer

For adoptive transfer, bone marrow neutrophils were purified from naïve WT and Sh2d1a$^{-/-}$ mice using Neutrophil Isolation Kit (Miltenei Biotech; cat. no. 130-097-658). Purified neutrophils were labeled separately with cell tracker orange CMRA dye (Invitrogen, cat. no. C34551), 5 μm for 10 min at 37 °C. Two million WT or sh2d1a$^{-/-}$ neutrophils labeled with the dye were administered intranasally into WT and sh2d1a$^{-/-}$ mice, undergoing pulmonary KPn infection for 2 days. After 4 h of transfer, BAL cells were isolated from each mouse cytocentrifuged on microscopic glass slides and fixed with 4% paraformaldehyde followed by Sytox Green nuclear staining (Thermo Fischer, cat. no. S7020, 100 nM). Images were acquired using Olympus IX83 TIRF Fluorescent Microscope and processed by ImageJ software. The percent NET formation was manually quantitated by dividing the number of the adoptively transferred (CMRA dye-labeled) NET-forming neutrophils by total number of adoptively transferred cells in 8–10 random microscopic fields and multiplying the values by 100.

Statistics

Statistical analysis of survival studies was performed by Kaplan–Meir log-rank test, bacterial burdens by Mann–Whitney U test (unpaired, nonparametric, two tailed), and adoptive transfer experiment by one-way ANOVA multiple-comparisons test. All other statistical analyses were performed using the Student's *t* test (GraphPad Prism 7.0 and SIGMA PLOT 8.0, Systat Software, San Jose, CA; $*p < 0.05$, $**p < 0.01$, $***p < 0.001$).

Supplementary data to this article can be found online at https://doi.org/10.1016/j.jmb.2019.07.002.

Acknowledgment

This work was supported by the National Institutes of Health (Grants R21AI107457 and R01AI121804 to J.S.; P20GM113123 to J.S. and B.B.M.). The flow cytometry core facility at UND is supported by INBRE and COBRE (Grants P20GM103442 and P20GM113123), and the imaging and histology core facilities are supported by COBRE (Grant P20GM113123) from the National Institutes of Health. The authors thank Dr. Steven Clegg, University of Iowa, for providing GFP-labeled *K. pneumoniae*. We also thank Ms. Sarah Abrahamson and Dr. Bryon Grove for technical assistance with imaging.

Conflict of Interest: The authors declare no financial conflict of interest.

Received 31 January 2019;
Received in revised form 19 June 2019;
Accepted 2 July 2019
Available online 08 July 2019

Keywords:
SLAM-associated protein, SAP, Sh2d1a;
NK1.1+ cells;
phagocytes;
neutrophils;
neutrophil extracellular traps

Abbreviations used:
NET, neutrophil extracellular trap; SLAM, signaling lymphocytic activation molecule; SAP, SLAM-associated protein; KO, knock-out; BAL, bronchoalveolar lavage; IF, immunofluorescence; BALF, cell-free bronchoalveolar lavage fluid; PMA, phorbol myristate acetate.

†Equal Contribution.

References

[1] G.S. Martin, D.M. Mannino, S. Eaton, M. Moss, The epidemiology of sepsis in the United States from 1979 through 2000, N. Engl. J. Med. 348 (2003) 1546–1554.

[2] F.B. Mayr, S. Yende, D.C. Angus, Epidemiology of severe sepsis, Virulence. 5 (2014) 4–11.

[3] M.E. Plazak, P.D. Tamma, E.L. Heil, The antibiotic arms race: current and emerging therapy for Klebsiella pneumoniae carbapenemase (KPC)-producing bacteria, Expert. Opin. Pharmacother. (2018) 1–13.

[4] M.J. Delano, P.A. Ward, The immune system's role in sepsis progression, resolution, and long-term outcome, Immunol. Rev. 274 (2016) 330–353.

[5] V. Papayannopoulos, Neutrophil extracellular traps in immunity and disease, Nat Rev Immunol. 18 (2018) 134–147.

[6] J.K. Tripathi, A. Sharma, P. Sukumaran, Y. Sun, B.B. Mishra, B.B. Singh, et al., Oxidant sensor cation channel TRPM2 regulates neutrophil extracellular trap formation and protects against pneumoseptic bacterial infection, FASEB J (2018), https://doi.org/10.1096/fj.201800605.

[7] C. Detre, M. Keszei, X. Romero, G.C. Tsokos, C. Terhorst, SLAM family receptors and the SLAM-associated protein (SAP) modulate T cell functions, Semin. Immunopathol. 32 (2010) 157–171.

[8] J.L. Cannons, L.J. Yu, B. Hill, L.A. Mijares, D. Dombroski, K.E. Nichols, et al., SAP regulates T(H)2 differentiation and PKC-theta-mediated activation of NF-kappaB1, Immunity. 21 (2004) 693–706.

[9] M. Verykokakis, M.D. Boos, A. Bendelac, B.L. Kee, SAP protein-dependent natural killer T-like cells regulate the development of CD8(+) T cells with innate lymphocyte characteristics, Immunity. 33 (2010) 203–215.

[10] H. Qi, From SAP-less T cells to helpless B cells and back: dynamic T–B cell interactions underlie germinal center development and function, Immunol. Rev. 247 (2012) 24–35.

[11] S.G. Tangye, XLP: clinical features and molecular etiology due to mutations in SH2D1A encoding SAP, J. Clin. Immunol. 34 (2014) 772–779.

[12] B.J. van Driel, G. Liao, P. Engel, C. Terhorst, Responses to microbial challenges by SLAMF receptors, Front. Immunol. 7 (2016) 4.

[13] C.N. Jondle, A. Sharma, T.J. Simonson, B. Larson, B.B. Mishra, J. Sharma, Macrophage galactose-type Lectin-1 deficiency is associated with increased neutrophilia and hyperinflammation in gram-negative pneumonia, J. Immunol. 196 (2016) 3088–3096.

[14] A. Sharma, A.L. Steichen, C.N. Jondle, B.B. Mishra, J. Sharma, Protective role of mincle in bacterial pneumonia by regulation of neutrophil mediated phagocytosis and extracellular trap formation, J. Infect. Dis. 209 (2014) 1837–1846.

[15] A.L. Steichen, B.J. Binstock, B.B. Mishra, J. Sharma, C-type lectin receptor Clec4d plays a protective role in resolution of gram-negative pneumonia, J. Leukoc. Biol. 94 (2013) 393–398.

[16] M.J. Delano, P.A. Ward, Sepsis-induced immune dysfunction: can immune therapies reduce mortality? J. Clin. Invest. 126 (2016) 23–31.

[17] J. Sharma, Q. Li, B.B. Mishra, M.J. Georges, J.M. Teale, Vaccination with an attenuated strain of Francisella novicida prevents T-cell depletion and protects mice infected with the wild-type strain from severe sepsis, Infect. Immun. 77 (2009) 4314–4326.

[18] J. Sharma, Q. Li, B.B. Mishra, J.M. Teale, Lethal pulmonary infection with Francisella novicida causes depletion of alphabeta T cells from lungs, Cell. Immunol. 257 (2009) 1–4.

[19] S. Latour, S. Winter, Inherited immunodeficiencies with high predisposition to Epstein–Barr virus-driven lymphoproliferative diseases, Front. Immunol. 9 (2018) 1103.

[20] S. Parolini, C. Bottino, M. Falco, R. Augugliaro, S. Giliani, R. Franceschini, et al., X-linked lymphoproliferative disease. 2B4 molecules displaying inhibitory rather than activating function are responsible for the inability of natural killer cells to kill Epstein–Barr virus-infected cells, J. Exp. Med. 192 (2000) 337–346.

[21] M. Ivin, A. Dumigan, F.N. de Vasconcelos, F. Ebner, M. Borroni, A. Kavirayani, et al., Natural killer cell-intrinsic type I IFN signaling controls Klebsiella pneumoniae growth during lung infection, PLoS Pathog. 13 (2017), e1006696.

[22] J.E. Boudreau, K.C. Hsu, Natural killer cell education and the response to infection and cancer therapy: stay tuned, Trends Immunol. 39 (2018) 222–239.

[23] S. Esin, G. Batoni, C. Counoupas, A. Stringaro, F.L. Brancatisano, M. Colone, et al., Direct binding of human NK cell natural cytotoxicity receptor NKp44 to the surfaces of mycobacteria and other bacteria, Infect. Immun. 76 (2008) 1719–1727.

[24] J. Voigt, K. Hunniger, M. Bouzani, I.D. Jacobsen, D. Barz, B. Hube, et al., Human natural killer cells acting as phagocytes against Candida albicans and mounting an inflammatory response that modulates neutrophil antifungal activity, J. Infect. Dis. 209 (2014) 616–626.

[25] S. Schmidt, L. Tramsen, B. Rais, E. Ullrich, T. Lehrnbecher, Natural killer cells as a therapeutic tool for infectious diseases—current status and future perspectives, Oncotarget. 9 (2018) 20891–20907.

[26] M.J. Czar, E.N. Kersh, L.A. Mijares, G. Lanier, J. Lewis, G. Yap, et al., Altered lymphocyte responses and cytokine production in mice deficient in the X-linked lymphoproliferative disease gene SH2D1A/DSHP/SAP, Proc. Natl. Acad. Sci. U. S. A. 98 (2001) 7449–7454.

[27] A.L. Steichen, T.J. Simonson, S.L. Salmon, D.W. Metzger, B.B. Mishra, J. Sharma, Alarmin function of galectin-9 in murine respiratory tularemia, PLoS One 10 (2015), e0123573.

[28] Y. Zhou, D.J. Schneider, E. Morschl, L. Song, M. Pedroza, H. Karmouty-Quintana, et al., Distinct roles for the A2B adenosine receptor in acute and chronic stages of bleomycin-induced lung injury, J. Immunol. 186 (2011) 1097–1106.

[29] A. Sharma, T.J. Simonson, C.N. Jondle, B.B. Mishra, J. Sharma, Mincle regulates autophagy to control neutrophil extracellular trap formation, J Infect Dis 215 (7) (2017) 1040–1048.

[30] B.B. Mishra, Q. Li, A.L. Steichen, B.J. Binstock, D.W. Metzger, J.M. Teale, et al., Galectin-3 functions as an alarmin: pathogenic role for sepsis development in murine respiratory tularemia, PLoS One 8 (2013), e59616.

[31] F.O. Quenum Zangbede, A. Chauhan, J. Sharma, B.B. Mishra, Galectin-3 in M2 macrophages plays a protective role in resolution of neuropathology in brain parasitic infection by regulating neutrophil turnover, J. Neurosci. 38 (2018) 6737–6750.